Chemical Science

ROYAL SOCIETY OF CHEMISTRY

EDGE ARTICLE

View Article Online
View Journal | View Issue

Check for updates

Cite this: *Chem. Sci.*, 2020, **11**, 5690

All publication charges for this article have been paid for by the Royal Society of Chemistry

# TIPS-pentacene triplet exciton generation on PbS quantum dots results from indirect sensitization†

Christopher M. Papa, [a] Sofia Garakyaraghi, [a] Devin B. Granger, [b] John E. Anthony [b] and Felix N. Castellano *[a]

Received 17th January 2020
Accepted 18th May 2020

DOI: 10.1039/d0sc00310g

rsc.li/chemical-science

Many fundamental questions remain in the elucidation of energy migration mechanisms across the interface between semiconductor nanomaterials and molecular chromophores. The present transient absorption study focuses on PbS quantum dots (QDs) of variable size and band-edge exciton energy (ranging from 1.15 to 1.54 eV) post-synthetically modified with a carboxylic acid-functionalized TIPS-pentacene derivative (TPn) serving as the molecular triplet acceptor. In all instances, selective excitation of the PbS NCs at 743 nm leads to QD size-dependent formation of an intermediate with time constants ranging from 2–13 ps, uncorrelated to the PbS QD valence band potential. However, the rate constant for the delayed formation of the TPn triplet excited state markedly increases with increasing PbS conduction band energy, featuring a parabolic Marcus free energy dependence in the normal region. These observations provide evidence of an indirect triplet sensitization process being inconsistent with a concerted Dexter-like energy transfer process. The collective data are consistent with the generation of an intermediate resulting from hole trapping of the initial PbS excited state by midgap states, followed by formation of the TPn triplet excited state whose rate constant and yield increases with decreasing quantum dot size.

Open Access Article. Published on 18 May 2020. Downloaded on 2/7/2026 1:02:23 PM.
This article is licensed under a Creative Commons Attribution-NonCommercial 3.0 Unported Licence.

## Introduction

Inorganic–organic hybrid materials constructed from semiconductor nanocrystals (NCs) with appended chromophoric molecules have found increasingly widespread use for a number of light-harvesting and light-emitting functions.[1–3] Most of these photonic processes rely on formally spin-triplet excited states, which are generally long-lived in organic molecules owing to their singlet ground states making radiative transitions spin-forbidden while possessing relatively low intrinsic spin–orbit coupling.[4,5] Meanwhile, triplet excited states are more easily accessed in inorganic semiconductor NCs due to their ill-defined (nearly isoenergetic) spin states following light absorption.[6] The earliest reports of triplet exciton transfer in such hybrid materials incorporated PbS or PbSe NCs coated with a thin film of tetracene or pentacene. These constructs relied on singlet fission[7,8] to generate triplet excitons in these molecular films that ultimately transferred to the NC triplet acceptors.[9,10] Subsequent to these reports, our laboratory discovered triplet–triplet energy transfer occurring in the reverse direction in toluene solutions featuring selectively photoexcited CdSe NCs with surface-anchored anthryl or pyrenyl molecules.[11] This investigation provided clear cut experimental evidence for direct Dexter-type energy transfer occurring across the CdSe quantum dot–molecule interface.[12]

However, PbS quantum dots, while unequivocally generating molecular triplet excitons following direct excitation of the NC,[13–16] have proven more mechanistically complex with respect to CdSe. Of particular importance was the identification of an unusual photogenerated reaction intermediate that appeared when 6,13-bis(triisopropylsilylethynyl)pentacene-2-carboxylic acid (TPn),[13] a closely related structural derivative of TIPS-pentacene, was anchored to the surface of PbS NCs. This observation was attributed to a sluggish hole trapping process that produced a charge separated state between PbS($e^-$) and $TPn^{\bullet+}$ and upon recombination generated the triplet excited state of TPn. A more recent account offered for PbS quantum dots' spectroscopically-observed deviation from traditional Dexter-type direct TTET relied on quantum chemical calculations to implicate a theoretical NC surface-localized excited state as the kinetic intermediate.[16]

To continue the mechanistic analysis of this hybrid system, four sizes of PbS NC were synthesized. Upon post-synthetic modification of the PbS NC surfaces with TPn, the sub-picosecond to supra-nanosecond dynamics of these systems were studied using transient absorption spectroscopy. Kinetic

[a]*Department of Chemistry, North Carolina State University, Raleigh, North Carolina 27695-8204, USA. E-mail: fncastel@ncsu.edu*

[b]*Department of Chemistry, University of Kentucky, Lexington, Kentucky 40506-0055, USA*

† Electronic supplementary information (ESI) available: Structural characterization of the PbS and PbS-TPn nanomaterials and additional transient absorption spectra and kinetic data and analyses. See DOI: 10.1039/d0sc00310g



This journal is © The Royal Society of Chemistry 2020

Open Access Article. Published on 18 May 2020. Downloaded on 2/7/2026 1:02:23 PM.
This article is licensed under a Creative Commons Attribution-NonCommercial 3.0 Unported Licence.

analysis of the experimental data indicates the conservation of a stepwise energy transfer mechanism from PbS NCs to TPn, irrespective to the size or band-gap energy of the NC. The rates of the second step in the stepwise mechanism suggest Marcus free energy dependence in the normal region. These results will be rationalized within the context of surface-trapped holes mediating triplet energy transfer.

# Experimental

### Nanomaterial synthesis and characterization

**Quantum dot syntheses.** Oleate-capped PbS NCs were synthesized by adapting previously reported procedures.[13,17] For the smallest PbS NC sizes, the sulfide precursor injection temperature was lowered from 110 °C to 95 °C for PbS-945 or 80 °C for PbS-805. While multiple batches per NC size were synthesized to ensure future synthetic reproducibility, all experiments (ligand exchanges, spectroscopy, and materials characterization) were performed on a single synthetic batch to eliminate batch-to-batch inhomogeneity. TPn was synthesized and structurally characterized as published previously.[18]

**Ligand exchange with TPn.** The oleate-capped PbS NCs were subjected to well established ligand exchange procedures.[11,13–16,19–21] Briefly, oleate-capped NCs were suspended in toluene to which TPn was added to initiate 1 : 1 X-type ligand exchange[15] with the oleate ligands. The NC-TPn hybrids were then purified by successive precipitation-centrifugation-resuspension and filtration steps. The average NC : TPn ratio was determined *via* UV-vis absorption spectroscopy. These values were found to be 1 : 20.7 for PbS-805-TPn, 1 : 33.2 for PbS-970-TPn, 1 : 42.3 for PbS-1000-TPn, and 1 : 53.9 for PbS-1075-TPn for time resolved spectroscopy samples.

**Static spectroscopy.** Electronic absorption spectra were measured on a Shimadzu UV-3600 UV-vis-NIR spectrophotometer. Steady-state photoluminescence spectra were measured on an Edinburgh Instruments FS920 fluorescence spectrometer equipped with both a visible and a near-infrared photomultiplier tube. Excitation at 743 nm was achieved by a 450 W Xe arc lamp equipped with a monochromator and appropriate long pass filters.

**Electron microscopy.** Transmission Electron Microscopy (TEM) experiments were carried out using a JEM 2000FX Scanning TEM (JEOL). Images were acquired at an accelerating voltage of 200 kV. Samples were prepared by evaporation of dilute NC suspensions in toluene that had been dropped onto an ultrathin carbon film on a lacey carbon support film on a 400 mesh Cu TEM grid. Size distributions were measured using ImageJ software (https://imagej.nih.gov/ij/). Particle sizing was done with the software's analyze particle function, after selection of an appropriate contrast threshold for the images. Scanning Electron Microscopy with Energy Dispersive X-ray Spectroscopy (SEM-EDS) was carried out on a FEI Verios 460L field-emission SEM (Thermo Fisher Scientific) equipped with a Si Drift Detector (Oxford Instruments). SEM-EDS samples were prepared by evaporation of dilute NC suspensions in toluene that had been dropped onto atomically smooth Si wafers.

### Time-resolved spectroscopic methods

**Ultrafast transient absorption spectroscopy.** Ultrafast transient absorption spectroscopy measurements were performed using an amplified Ti:sapphire laser system described previously in the literature.[22] Briefly, the output from a Coherent Libra 1 kHz Ti:sapphire regenerative amplifier (4 mJ per pulse, 100 fs fwhm at 800 nm) was split into pump and probe beams. The pump beam was directed into an optical parametric amplifier (Coherent OPerA Solo) to generate tunable excitation (743 nm) while the probe beam was delayed in a 6.2 ns optical delay stage before being broadened by a nonlinear optical crystal into broadband white light (sapphire to generate the probe light for visible TA or a proprietary crystal to generate the probe light for NIR TA) before passing through the sample. The two beams were focused and spatially overlapped with the relative polarization of the pump and probe beams set to the magic angle of 54.7°. NC suspensions were measured in 2 mm path length quartz cuvettes and stirred constantly to alleviate local heating from the laser pulses. The PbS and PbS-TPn solutions were prepared to possess optical densities (OD) of approximately 0.06 at 743 nm. The transient absorption difference spectra and kinetics were obtained using a Helios transient absorption spectrometer (Ultrafast Systems), averaging four scans and using 2 s of averaging at every given delay. The ground state absorption spectra were taken before and after each experiment using an Agilent 8453 UV-visible spectrophotometer to ensure there was no sample decomposition.

**Nanosecond transient absorption spectroscopy.** Nanosecond TA measurements were executed using a LP920 spectrometer (Edinburgh Instruments). An iStar ICCD camera (Andor Technology) was used to obtain transient difference spectra. Single-wavelength kinetics were collected on either a visible light PMT or an InGaAs photodiode for NIR detection. The excitation source was a tunable Vibrant 355 Nd:YAG/OPO system (OPOTEK) tuned to 743 nm (1 mJ per pulse, 5–7 ns fwhm). While this excitation power is sufficient to generate multiple excitons in PbS NCs, multiexciton processes such as biexciton and triexciton annihilation are expected to be significantly shorter-lived than the pulse duration (5–7 ns fwhm). The excitation source operated at 1 Hz and 3.3 Hz for spectra and kinetics acquisitions, respectively. Appropriate long pass filters were used to remove residual leaking light from the excitation source. The samples were deaerated by a minimum of three freeze–pump–thaw degassing cycles. The PbS and PbS-TPn samples were diluted to OD of approximately 0.06 at 743 nm.

**Extracting kinetic rate constants from transient absorption spectra.** Ultrafast transient absorption (TA) spectra were fit using a model based on the assumption that the time-resolved TA spectra of these hybrid materials can be linearly decomposed as the sum of time-independent decay-associated difference spectra (DADS) with specific time-dependent amplitudes.[23] Under this assumption, each DADS is therefore presumed to represent the TA spectrum of an individual excited state in the system. The time-dependent amplitudes correspond to the concentration or population of their respective DADS. In solving for these values from the PbS-TPn TA data, each DADS was

Open Access Article. Published on 18 May 2020. Downloaded on 2/7/2026 1:02:23 PM.
This article is licensed under a Creative Commons Attribution-NonCommercial 3.0 Unported Licence.

assumed to interconvert to the next in a sequential, first order fashion.

Three DADS and an additional fitting parameter could model the complete ultrafast TA spectral datasets for all PbS-TPn materials studied. The additional fitting parameter, resembling a fourth DADS, is included in the model to account for a nonlinear response feature from the toluene occurring coincidentally with the impulse response function (IRF). The spectra produced by the model appear in Fig. 3a–d. Additionally, the fits obtained from the model are compared to the experimental data at the end of the ESI (Fig. S12–S19).† The PbS-TPn TA data was fit separately for the individual white light continua in the visible and NIR, respectively, and the corresponding rate constants were found to be in excellent agreement. The kinetic rate constants extracted from the model have been used to interpret the experimental data (Table S3†).

## Results and discussion

The four sizes of PbS NC that were synthesized are displayed in Fig. 1a and b. Consistent with quantum-confined semiconductor nanomaterials, the lowest energy PbS NC exciton absorbance maximum shifts to higher energies with decreasing PbS NC average diameter,[24–27] supported by analysis of TEM images (Fig. S1†). The wavelength of maximum photoluminescence intensity shifts in concert with the maximum absorbance wavelength in the first exciton band. The PbS NCs possess photoluminescence intensity maxima near 805, 970, 1000, and 1075 nm, and will be referred to as PbS-805, PbS-970, PbS-1000, and PbS-1075.

As a representative example of the change in electronic effects upon surface-functionalization, the absorption and photoluminescence spectra for PbS-1075 before and after ligand exchange of oleate to TPn and subsequent purification are given in Fig. 1c. The absorption spectrum of free TPn is included for reference. The corresponding spectra for all other hybrid materials subjected to TA spectroscopy are presented in Fig. S2.† While the colloidal NC ligand exchange process and its specific effects in the context of time-resolved optical spectroscopy has been discussed at length elsewhere,[11,13–16,19–21] a subtle spectral feature is noteworthy here. In all four discrete materials investigated, a red shift of the TPn absorption bands was consistently observed, often accompanied by a blue shift of the PbS first exciton band. TEM images taken after ligand exchange (Fig. S3†) showed no change in PbS NC average particle size. In the PbS-805 hybrid materials, spectral congestion from the energetic similarity between the PbS first exciton absorbance band and the TPn absorbance band prohibits definitive assignment of the concomitant PbS absorption blue shift. These shifts are reminiscent of NC-molecule electronic wavefunction interactions that occur in strongly quantum-confined materials.[13,28]

TA spectroscopy was utilized to interrogate the excited state dynamics occurring in the oleate-capped PbS NCs. Fig. 2a displays time dependent TA difference spectra for PbS-805 suspended in toluene using a visible light probe (430–780 nm) following 743 nm pulsed laser excitation (0.15 μJ per pulse, 100 fs fwhm, 0.8 excitations per NC). This excitation wavelength was chosen because it is absorbed by all four NC species but not by TPn, therefore allowing all hybrid materials to achieve selective PbS excitation at a single wavelength. Pumping a solution of TPn without any PbS NCs at 743 nm results in no discernible TA signals (Fig. S4†), indicating that the PbS NCs are selectively excited at this wavelength. Visible and near-IR (830–1380 nm) TA difference spectra for solutions of PbS-1075, PbS-1000, PbS-970, PbS-805 following 743 nm pulsed laser excitation are presented in Fig. S5,† All four PbS species display a prompt, characteristic negative polarity absorption feature, associated with bleaching of their first exciton absorption band. PbS-805 is instructive to illustrate the general excited-state spectral signatures of PbS NCs. This is because the negative polarity TA signal for the PbS-805 first exciton bleach appears within the same

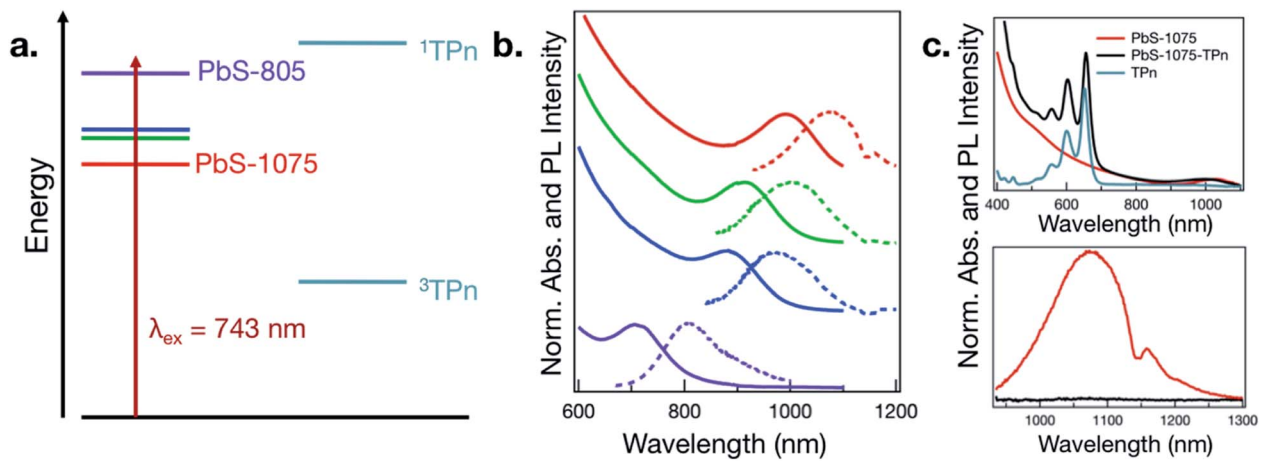


Fig. 1 (a) Illustration of PbS nanocrystal first exciton and TPn-centered energy levels. (b) Electronic absorption (solid lines) and emission spectra (dashed lines) for PbS NCs ranging in diameter from 3.3 nm (top, red) to 2.2 nm (bottom, violet). (c) Electronic absorption spectra (top) in toluene of PbS-1075 nanocrystals before and after ligand exchange by TPn with free TPn shown, and photoluminescence spectra in toluene (bottom) of PbS-1075 and PbS-1075-TPn. The depression in the photoluminescence near 1150 nm results from toluene absorption.

 This journal is © The Royal Society of Chemistry 2020

Open Access Article. Published on 18 May 2020. Downloaded on 2/7/2026 1:02:23 PM.
This article is licensed under a Creative Commons Attribution-NonCommercial 3.0 Unported Licence.

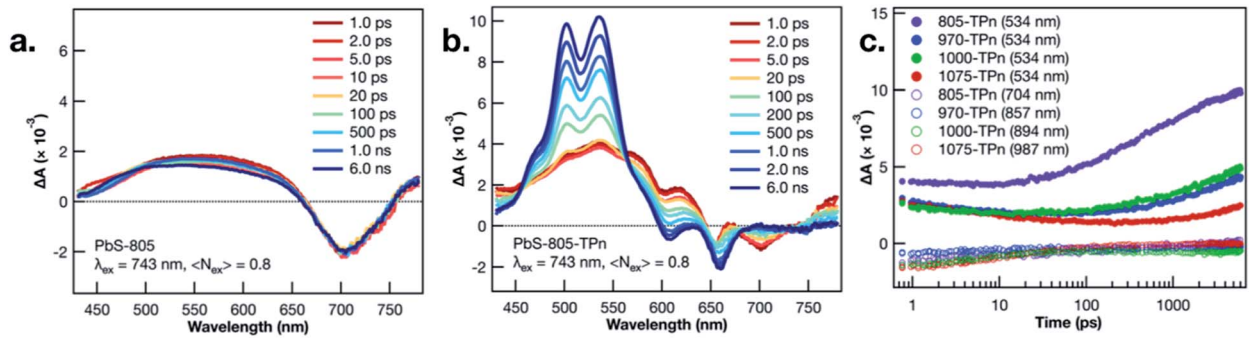


Fig. 2 Ultrafast TA difference spectra of PbS-805 (a) and PbS-805-TPn (b) suspensions in toluene following 743 nm pulsed laser excitation (0.15 μJ per pulse, 100 fs fwhm). Time delays range from 1.0 ps (red) to 6.0 ns (blue). Ultrafast TA kinetics (c) probed at 534 nm (closed circles) and different PbS first exciton bleach wavelengths (open circles) for PbS-805-TPn (purple), PbS-970-TPn (blue), PbS-1000-TPn (green), and PbS-1075-TPn (red) suspensions in toluene following 743 nm pulsed laser excitation (0.15 μJ per pulse, 100 fs fwhm).

visible region of the electromagnetic spectrum as the other notable PbS-TPn excited state features. These PbS-TPn features consist of the broad induced absorption band characteristic of interband transitions in the excited PbS NCs[29–32] and some notable TPn transient spectral features. Over the maximum probe delay of the ultrafast TA measurements (6.2 ns), all four PbS TA difference spectra remain mostly unchanged. Nanosecond TA experiments (Fig. S6 and S7†) feature symmetric decay of PbS excited state spectral features on a 1–2 μs time scale. These results are consistent with extant knowledge of the excited state dynamics of carboxylate-capped PbS NCs.[13,15,16,32–45]

Following PbS NC surface functionalization with TPn molecules, the TA difference spectra and kinetics following selective excitation of the NCs are changed significantly (Fig. 2b and S8†). Upon pulsed laser excitation at 743 nm, the initially formed excited state resembles the excited state of the oleate-capped PbS NCs with the added presence of three negative absorption features at 550, 600, and 650 nm superimposed on the broad PbS excited state. The location of the negative features implies a relationship to the ground state absorption spectrum of TPn. These negative features have been previously assigned[13] and independently reproduced in a closely related study[16] as a transient dipole-induced shift of the $S_0$ to $S_1$ electronic transitions in TPn.[46–50] In PbS-1075-TPn, the material most analogous to those studied previously,[13,16] the first exciton absorption band bleach disappears over the first 250 ps after excitation. Concomitantly, the broad PbS excited state absorbance was observed to symmetrically attenuate. This was followed by the growth of a band centered at 530 nm, previously assigned to the PbS-bound molecular triplet $^3$TPn.[13,16] The molecular triplet develops with a time constant of roughly 8 ns, in stark contrast to the ps-regime decays of the spectral features associated with the PbS NC excited state, but in universal agreement with previous related studies.[13,16] The assignments and temporal ordering of the time-resolved spectral features for all PbS NC hybrid materials, regardless of size, are consistent with the same mechanism. This mechanism consists of a decay of the PbS NC excited state on ps time scales to a kinetic intermediate[13,16] followed by a nanosecond time scale growth of the TPn excited triplet state.

In all four TPn-modified materials, the time constants for the observed decay of the NIR bleach features were coterminous with the decays of the broad visible absorption features (Table S1†). PbS-805-TPn (Fig. S8a†) is of particular interest to this study because the first exciton bleach is now contained in the region probed by the same visible white light generating crystal. This enables comparison of the dominant $^3$TPn signal at 534 nm with the PbS NC first exciton bleach at 710 nm. Furthermore, the shift of the bleach wavelength decongests the NIR white light continuum for observation of the $^3$TPn signal at 994 nm and a characteristic $TPn^{\bullet+}$ signal expected near 876 nm.[21] The $^3$TPn signal at 994 nm appears in TA difference spectra for PbS-1000-TPn, PbS-970-TPn, and PbS-805-TPn following 743 nm pulsed laser excitation on time scales matching the growth of the $^3$TPn feature around 530 nm (Fig. S8b, d and f†). However, the $TPn^{\bullet+}$ signal expected near 876 nm is not observed in PbS-1000-TPn or PbS-970-TPn at any time point. There is a feature observed at 876 nm in PbS-805-TPn on the same time scale as the $^3$TPn features at 530 nm and 994 nm. This kinetic behaviour is indicative that the $TPn^{\bullet+}$ formed is unlikely to be acting as the primary kinetic intermediate to $^3$TPn formation. The decay rates of the characteristic PbS NC excited state features all increased with increasing PbS NC first exciton energy, as did the growth rates of $^3$TPn (Fig. 2c). The TA difference spectra and kinetics for the PbS-TPn materials on supra-nanosecond time scales (Fig. S9 and S10†) illustrate symmetric decay of the NC-appended $^3$TPn spectral features on microsecond time scales (Table S2†). The time constants associated with this excited state relaxation process approach the time constant for the relaxation of freely diffusing $^3$TPn as the PbS NCs decrease in diameter.[13] The observed trend in $^3$TPn lifetime as a function of PbS NC size is consistent with a concentration effect[15] induced by the greater number of TPn molecules that can be accommodated by the larger NCs. Temperature-dependent decay kinetics of the $^3$TPn TA signals (Fig. S11†) indicate the reduction in lifetime is unlikely to be a thermally activated excited state process, as previously observed in other NC-molecule materials featuring reverse triplet–triplet energy transfer.[19,20] The lack of experimental evidence supporting any reverse TTET occurring at these

Open Access Article. Published on 18 May 2020. Downloaded on 2/7/2026 1:02:23 PM.
This article is licensed under a Creative Commons Attribution-NonCommercial 3.0 Unported Licence.

interfaces remains inconsistent with a concerted Dexter-like process.

In the interest of assigning consistent rate constants to the three excited state processes occurring in each material, we used a spectral decomposition model[23] (*vide supra*) to fit the time-resolved TA difference spectra. The three decay-associated difference spectra (DADS) fit to the model of the PbS-1075-TPn data collected over the first 6.2 ns after pulsed 743 nm excitation are displayed in Fig. 3a. The first DADS (dark red) is reminiscent of the spectrum observed immediately upon selective excitation of the PbS NC. Specifically, it contains a PbS first exciton bleach in the NIR combined with a broadband PbS induced absorption in the visible with the three negative absorption features from the transient dipole-induced TPn absorption shift. Meanwhile, the third DADS (Fig. 3a, pink) is a strong match to the spectrum of the PbS-appended $^3$TPn species from the final ultrafast TA time delay and the prompt nanosecond TA difference spectra (Fig. S8g, h and S9d†). The first DADS evolves into the second DADS (Fig. 3a, red) with a time constant of 12.6 ps. Subsequently, the second DADS evolves into the third with a time constant of 8.0 ns. Both time constants are in good agreement with single-wavelength kinetic analyses of the experimental data and previously published results.[13,16] Consistent with the single wavelength kinetic analyses, three sequential DADS model the TA difference spectra in every PbS-TPn species investigated here. The sub-microsecond time constants for the PbS-TPn materials extracted from the model are summarized in Table S3.† The final step to obtain consistent rate constants for the two sub-microsecond excited state processes was to average the rate constants on an average TPn per PbS NC basis, which are also included in Table S3.†

Recent work on $CuInS_2$ NCs has magnified the existence of charge-carrier trapping phenomena in semiconductor NCs, specifically with respect to energy transfer across the NC-molecule interface.[51] In the related PbS-acene study by Bender, Raulerson *et al.*, electronic structure calculations provide a rationale for the existence of surface-localized excited states on the PbS NC.[16] A direct comparison of the triplet sensitization of two different acene molecules by $CsPbBr_3$ NCs suggested that electrons and holes could possess vastly different trapping kinetics.[52] The calculated PbS NC surface states were previously tentatively assigned to hole-trapping phenomena at the NC surface.[16] A plausible next step toward validating that mechanistic assignment would be to study the NC size-dependence of triplet–triplet energy transfer from multiple sizes of PbS NC to pentacene. This is the first such PbS NC to acene triplet–triplet energy transfer NC-size-dependence study to employ either NC-selective excitation or a pentacene derivative as the acceptor. If the kinetic intermediate, which is observed comprehensively across all PbS NC sizes investigated, is a surface hole-trapping phenomenon, that could explain the absence of $TPn^{\bullet+}$ TA signals discussed earlier. Furthermore, we propose this mechanism provides a suitable explanation for the size-dependent behaviour of the $^3$TPn TA signal growth rates displayed in Fig. 3e. The rate constants for formation of the $^3$TPn state increase with increasing PbS conduction band position, featuring a parabolic Marcus free energy dependence in the normal region. As mentioned previously, the rate constants on the vertical axis in Fig. 3e have been adjusted to reflect the differing surface concentrations of TPn on the different sizes of the PbS NC. However, they do not account for any changes in NC-TPn electronic coupling as a function of PbS NC size. Taking these factors into account, the fit applied to the data herein was intended primarily as a phenomenological guide to the eye. However, the values extracted from the fit in this study are broadly consistent with recently reported data

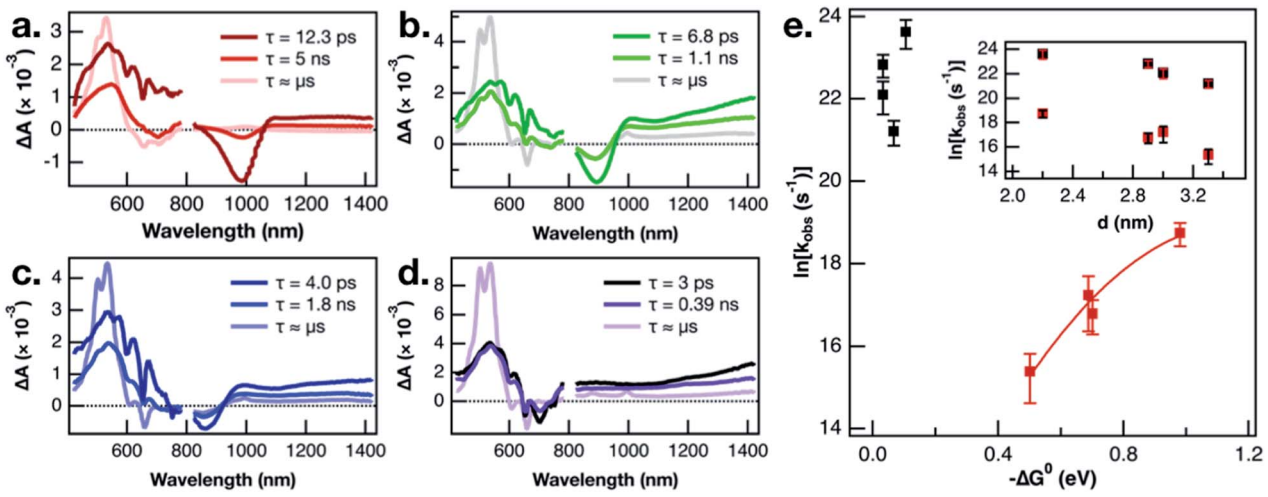


Fig. 3 Basis spectra modeled on TA spectra of (a) PbS-1075-TPn, (b) PbS-1000-TPn, (c) PbS-970-TPn, and (d) PbS-805-TPn materials. The ultrafast TA spectra initially resemble the 1st (darkest hues) spectra and eventually come to resemble the 3rd spectra (palest hues) by the end of the 6.2 ns delay stage. The 2nd spectra (intermediate hues) are necessary to accurately model the experimental data. Data from 425 to 775 nm and data from 825 to 1325 nm were fit with matching rate constants. Logarithm of extracted rate constants plotted as a function of thermodynamic driving force (e) and approximate PbS NC diameter ((e), inset). Bars in (e) and ((e), inset) reflect the standard error calculated from three independent measurements. The solid red line in (e) is a Marcus theory fit to the data intended as a phenomenological guide for the eye.

 This journal is © The Royal Society of Chemistry 2020

Open Access Article. Published on 18 May 2020. Downloaded on 2/7/2026 1:02:23 PM.
This article is licensed under a Creative Commons Attribution-NonCommercial 3.0 Unported Licence.

from a PbS QD and tetracene study which also employed a fit to Marcus theory.[53] Meanwhile, the rate constants associated with the attenuation of the initial PbS NC excited state are not well-predicted by Marcus theory. As shown in the inset of Fig. 3e, the PbS NC size-dependence of the rate constants for decay of the PbS excited state appears to be directly related to the NC diameter. We suggest the rate constants for this first step deviate from Marcus theory in part because they are intrinsic to the PbS NCs or otherwise independent from the energetics of TPn. The combination of the current size and band gap kinetic dependence data, the recent work on charge carrier trapping,[51,52] and the theoretical evidence for surface state mediation,[16] supports a hole-trapping mechanism for $^3$TPn generation from excited PbS NCs. On picosecond time scales, surface state trapping of photogenerated holes quenches the PbS band edge exciton, while $^3$TPn is directly generated from the hole-trapped PbS NC much more slowly.

## Conclusions

We have functionalized a series of PbS NCs with TPn, a derivative of TIPS-pentacene, to generate a suite of hybrid inorganic–organic nanomaterials. We have investigated these nanomaterials from sub-picosecond to supra-nanosecond time scales using transient absorption spectroscopy in the visible and near-IR portions of the electromagnetic spectrum. Selective photoexcitation of PbS NCs produces a kinetic intermediate over picosecond time scales, which decays to yield TPn-localized triplet excitons on nanosecond time scales. This stepwise triplet sensitization process is comprehensive across all PbS NC sizes and band-edge exciton energies investigated. The evidence is demonstrative of stepwise (indirect) sensitization and inconsistent with a concerted Dexter-like process. This work demonstrates the inherent complexity in the interactions between direct energy transfer processes, semiconductor trap states, and stepwise electron transfers. Understanding these interactions is fundamental to successfully govern directional triplet energy transfer or sensitization from semiconductor NCs to surface-appended molecules.

## Conflicts of interest

There are no conflicts to declare.

## Acknowledgements

We acknowledge support for this work from the Organic Materials Chemistry program in the Air Force Office of Scientific Research (FA9550-18-1-0331). Electron microscopy was performed at the Analytical Instrumentation Facility (AIF) at North Carolina State University, which is supported by the State of North Carolina and the National Science Foundation (Award Number ECCS-1542015). The AIF is a member of the North Carolina Research Triangle Nanotechnology Network (RTNN), a site in the National Nanotechnology Coordinated Infrastructure (NNCI).

## References

1 Z. Huang and M. Lee Tang, *J. Phys. Chem. Lett.*, 2018, **9**, 6198–6206.
2 S. Garakyaraghi and F. N. Castellano, *Inorg. Chem.*, 2018, **57**, 2351–2359.
3 H. Lu, G. M. Carroll, N. R. Neale and M. C. Beard, *ACS Nano*, 2019, **13**, 939–953.
4 N. J. Turro, *Modern Molecular Photochemistry*, 1991.
5 A. Olaya-Castro and G. D. Scholes, *Int. Rev. Phys. Chem.*, 2011, **30**, 49–77.
6 G. D. Scholes, *Adv. Funct. Mater.*, 2008, **18**, 1157–1172.
7 M. B. Smith and J. Michl, *Chem. Rev.*, 2010, **110**, 6891–6936.
8 M. B. Smith and J. Michl, *Annu. Rev. Phys. Chem.*, 2013, **64**, 361–386.
9 M. Tabachnyk, B. Ehrler, S. Gelinas, M. L. Boehm, B. J. Walker, K. P. Musselman, N. C. Greenham, R. H. Friend and A. Rao, *Nat. Mater.*, 2014, **13**, 1033–1038.
10 N. J. Thompson, M. W. B. Wilson, D. N. Congreve, P. R. Brown, J. M. Scherer, T. S. Bischof, M. Wu, N. Geva, M. Welborn, T. Van Voorhis, V. Bulovic, M. G. Bawendi and M. A. Baldo, *Nat. Mater.*, 2014, **13**, 1039–1043.
11 C. Mongin, S. Garakyaraghi, N. Razgoniaeva, M. Zamkov and F. N. Castellano, *Science*, 2016, **351**, 369–372.
12 D. L. Dexter, *J. Chem. Phys.*, 1953, **21**, 836–850.
13 S. Garakyaraghi, C. Mongin, D. B. Granger, J. E. Anthony and F. N. Castellano, *J. Phys. Chem. Lett.*, 2017, **8**, 1458–1463.
14 Z. Huang, Z. Xu, M. Mahboub, X. Li, J. W. Taylor, W. H. Harman, T. Lian and M. L. Tang, *Angew. Chem., Int. Ed.*, 2017, **56**, 16583–16587.
15 D. M. Kroupa, D. H. Arias, J. L. Blackburn, G. M. Carroll, D. B. Granger, J. E. Anthony, M. C. Beard and J. C. Johnson, *Nano Lett.*, 2018, **18**, 865–873.
16 J. A. Bender, E. K. Raulerson, X. Li, T. Goldzak, P. Xia, T. Van Voorhis, M. L. Tang and S. T. Roberts, *J. Am. Chem. Soc.*, 2018, **140**, 7543–7553.
17 M. A. Hines and G. D. Scholes, *Adv. Mater.*, 2003, **15**, 1844–1849.
18 Z. Li, K. Shankar, G. K. Mor, R. A. Grimminger, C.-M. Lin, J. E. Anthony and C. A. Grimes, *J. Photonics Energy*, 2011, **1**, 011106.
19 C. Mongin, P. Moroz, M. Zamkov and F. N. Castellano, *Nat. Chem.*, 2018, **10**, 225–230.
20 M. La Rosa, S. A. Denisov, G. Jonusauskas, N. D. McClenaghan and A. Credi, *Angew. Chem., Int. Ed.*, 2018, **57**, 3104–3107.
21 H. P. Lu, X. H. Chen, J. E. Anthony, J. C. Johnson and M. C. Beard, *J. Am. Chem. Soc.*, 2019, **141**, 4919–4927.
22 S. Garakyaraghi, E. O. Danilov, C. E. McCusker and F. N. Castellano, *J. Phys. Chem. A*, 2015, **119**, 3181–3193.
23 L. J. G. W. van Wilderen, C. N. Lincoln and J. J. van Thor, *PLoS One*, 2011, **6**, e17373.
24 P. Kambhampati, *Acc. Chem. Res.*, 2011, **44**, 1–13.
25 D. B. Turner, Y. Hassan and G. D. Scholes, *Nano Lett.*, 2012, **12**, 880–886.

Open Access Article. Published on 18 May 2020. Downloaded on 2/7/2026 1:02:23 PM.
This article is licensed under a Creative Commons Attribution-NonCommercial 3.0 Unported Licence.

26 K. J. Schnitzenbaumer, T. Labrador and G. Dukovic, *J. Phys. Chem. C*, 2015, **119**, 13314–13324.
27 M. S. Azzaro, M. C. Babin, S. K. Stauffer, G. Henkelman and S. T. Roberts, *J. Phys. Chem. C*, 2016, **120**, 28224–28234.
28 H. Zhu, Y. Yang, K. Hyeon-Deuk, M. Califano, N. Song, Y. Wang, W. Zhang, O. V. Prezhdo and T. Lian, *Nano Lett.*, 2014, **14**, 1263–1269.
29 P. Kambhampati, *Chem. Phys.*, 2015, **446**, 92–107.
30 V. I. Klimov, in *Annual Review of Physical Chemistry*, 2007, vol. 58, pp. 635–673.
31 B. Cho, W. K. Peters, R. J. Hill, T. L. Courtney and D. M. Jonas, *Nano Lett.*, 2010, **10**, 2498–2505.
32 Y. Yang, W. Rodriguez-Cordoba and T. Lian, *J. Am. Chem. Soc.*, 2011, **133**, 9246–9249.
33 H. Du, C. L. Chen, R. Krishnan, T. D. Krauss, J. M. Harbold, F. W. Wise, M. G. Thomas and J. Silcox, *Nano Lett.*, 2002, **2**, 1321–1324.
34 B. L. Wehrenberg, C. J. Wang and P. Guyot-Sionnest, *J. Phys. Chem. B*, 2002, **106**, 10634–10640.
35 J. H. Warner, E. Thomsen, A. R. Watt, N. R. Heckenberg and H. Rubinsztein-Dunlop, *Nanotechnology*, 2005, **16**, 175–179.
36 S. W. Clark, J. M. Harbold and F. W. Wise, *J. Phys. Chem. C*, 2007, **111**, 7302–7305.
37 Y. Chen, D. Yu, B. Li, X. Chen, Y. Dong and M. Zhang, *Appl. Phys. B: Lasers Opt.*, 2009, **95**, 173–177.
38 M. S. Gaponenko, A. A. Lutich, N. A. Tolstik, A. A. Onushchenko, A. M. Malyarevich, E. P. Petrov and K. V. Yumashev, *Phys. Rev. B*, 2010, **82**, 125320.
39 K. E. Knowles, M. Malicki and E. A. Weiss, *J. Am. Chem. Soc.*, 2012, **134**, 12470–12473.
40 Y. Yang, W. Rodriguez-Cordoba and T. Lian, *Nano Lett.*, 2012, **12**, 4235–4241.
41 Y. Yang, W. Rodriguez-Cordoba, X. Xiang and T. Lian, *Nano Lett.*, 2012, **12**, 303–309.
42 Y. Yang and T. Lian, *Coord. Chem. Rev.*, 2014, **263**, 229–238.
43 K. O. Aruda, M. B. Kunz, M. Tagliazucchi and E. A. Weiss, *J. Phys. Chem. Lett.*, 2015, **6**, 2841–2846.
44 H. Chung, H. Choi, D. Kim, S. Jeong and J. Kim, *J. Phys. Chem. C*, 2015, **119**, 7517–7524.
45 M. Wu, D. N. Congreve, M. W. B. Wilson, J. Jean, N. Geva, M. Welborn, T. Van Voorhis, V. Bulovic, M. G. Bawendi and M. A. Baldo, *Nat. Photonics*, 2016, **10**, 31–34.
46 L. Sebastian, G. Weiser and H. Bassler, *Chem. Phys.*, 1981, **61**, 125–135.
47 D. J. Norris, A. Sacra, C. B. Murray and M. G. Bawendi, *Phys. Rev. Lett.*, 1994, **72**, 2612–2615.
48 G. U. Bublitz and S. G. Boxer, *Annu. Rev. Phys. Chem.*, 1997, **48**, 213–242.
49 S. Ardo, Y. Sun, F. N. Castellano and G. J. Meyer, *J. Phys. Chem. B*, 2010, **114**, 14596–14604.
50 S. Gelinas, A. Rao, A. Kumar, S. L. Smith, A. W. Chin, J. Clark, T. S. van der Poll, G. C. Bazan and R. H. Friend, *Science*, 2014, **343**, 512–516.
51 Y. Han, S. He, X. Luo, Y. Li, Z. Chen, W. Kang, X. Wang and K. Wu, *J. Am. Chem. Soc.*, 2019, **141**, 13033–13037.
52 X. Luo, Y. Y. Han, Z. W. Chen, Y. L. Li, G. J. Liang, X. Liu, T. Ding, C. M. Nie, M. Wang, F. N. Castellano and K. F. Wu, *Nat. Commun.*, 2020, **11**, 28.
53 V. Gray, J. R. Allardice, Z. Zhang, S. Dowland, J. Xiao, A. J. Petty, J. E. Anthony, N. C. Greenham and A. Rao, *ACS Nano*, 2020, **14**, 4224–4234.


This journal is © The Royal Society of Chemistry 2020